

# Design of a Kinetic Energy Harvester for Elephant Mounted Wireless Sensor Nodes of JumboNet

Malitha Wijesundara<sup>\*†</sup>, Cristiano Tapparello\*, Amalinda Gamage<sup>‡</sup>, Yadhavan Gokulan<sup>‡</sup>,  
Logan Gittelson<sup>†</sup>, Thomas Howard\*, Wendi Heinzelman\*

\*Department of Electrical and Computer Engineering, University of Rochester, Rochester, NY

†Department of Computer Science, University of Rochester, Rochester, NY

‡Department of Information Systems Engineering, Sri Lanka Institute of Information Technology, Sri Lanka

\*{mwijesun,ctappare,thoward,wheinzel}@ece.rochester.edu, †lgittels@cs.rochester.edu,

‡{malitha.w,amalinda.j,yadhavan.g}@slit.lk

**Abstract**—In areas where the habitats of elephants and humans are rapidly encroaching on each other, real-time monitoring of the elephants' locations has the potential to drastically improve the co-existence of elephants and humans, resulting in reduced deaths in both groups. However, as tagging (using GPS collars) elephants to obtain such location information is difficult and costly, it is important to ensure very long lifetimes of the tags, which can only be achieved using energy harvesting. In this paper, we present a kinetic energy harvester that uses magnetic levitation and ferro fluid bearings to generate energy from an elephant's movements. In order to determine the feasibility of using this kinetic energy harvester for powering the tags on elephants, we obtained real acceleration data collected from an Asian elephant over a 10 day period, and this data was then used to tune the system to maximize the harvested energy. Using experimentally validated analytical and simulation models, and the actual elephant acceleration data, we find that our prototype can generate 88.91J of energy per day. This energy is not only sufficient to power the tags to acquire and transmit locations 24 times a day to a distance of 114km (line of sight), but provides a surplus of at least 35.40J, which can be used to increase the frequency of position updates or to support alternative communication options such as GPRS. Therefore, this shows the viability of long-term tracking of elephants.

## I. INTRODUCTION

Since 1986, the Asian Elephant (*Elephas maximus*) has been listed as endangered by the International Union for Conservation of Nature (IUCN) due to a 50% reduction in population over the last 50-75 years [1]. According to IUCN, the greatest threats to the Asian elephant are loss, degradation, and fragmentation of habitat due to expanding human population. This in-turn leads to increasing conflicts between humans and elephants.

The Sri Lankan elephant (*Elephas maximus maximus*) is one of three recognized subspecies of the Asian elephant and is the largest in size. The total elephant population in Sri Lanka stood at 5,879 in 2011, according to the Department of Wild Life in Sri Lanka. On average, more than 200 elephants and more than 70 people are killed annually as a result of conflicts between elephants and humans in Sri Lanka alone [2].

The search for effective measures to deal with Human-Elephant Conflicts (HEC) is one of the most significant challenges for elephant conservation globally. Real-Time Monitoring (RTM) of positional data using tracking units attached

to animals is emerging as an effective tool for ecological monitoring and wild life conservation. As an example, Wall et al. [3] have performed real-time monitoring of proximity, geofencing, movement rate and immobility detection on 94 elephants to prove its effectiveness compared with traditional slow and often inaccurate monitoring techniques. Their system is composed of an elephant-mounted collar that uses satellite and GSM networks to transmit GPS and auxiliary sensor data to a cloud based storage where analysis is performed and necessary alerts are generated within 5 minutes. In their study, the collar is powered by a 130Ah battery and, when acquiring data once every hour, it is able to run for about 600 days [3]. While this represents a viable solution to monitor wild elephants, the large battery used by this study adds substantial weight to the collar ( $\sim 5\text{Kg}$ ), and can be dangerous to the animal due to overheating and potential explosion.

Given the cost and the effort of collaring an elephant, as well as the possible risks of attaching electrical devices to animals, it is desirable to use limited size and weight devices, combined with suitable energy harvesting techniques that would recharge small size batteries. This has three advantages; 1) having a system that is safer and less intrusive on the elephants, 2) the availability of a higher amount of energy to support longer distances and more frequent transmissions, and 3) the extended lifetime of the collars.

The declining cost of solar panels makes harvesting solar energy a viable solution for energy harvesting in Wireless Sensor Networks (WSNs). Solar energy harvesting has been successfully implemented in animal monitoring such as, for example, in ZebraNet [4] and TurtleNet [5] for monitoring zebras and turtles, respectively. However, solar energy harvesting has several limitations in animal tracking depending on the location, the environment and the behavior of the animal to be tracked. As an example, Asian elephants prefer to be under shade during midday and often cover themselves with mud and dirt to insulate themselves from the sun. Moreover, due to their nocturnal behavior, a significantly higher number of deaths and injuries occur during the night and early mornings when elephants encroach on human habitats.

The motion of an Asian elephant in a zoo was recorded and categorized in [6], where the sensors used in this study

recorded some bodily motion at all times of the day, with the exception of 17-31% of the time when the elephant was stationary (sleeping). In addition, recent studies on wild elephants showed that, on average, Asian elephants travel 3.2 km per day as herds, while lone males travel 3.6 km per day and up to 8.9 km per day in musth [7]. This continuous movement provides opportunities for kinetic energy harvesting, which could be considered as an alternative to solar energy harvesting. In fact, the design of a kinetic energy harvester for cattle monitoring is presented in [8]. This harvester has two coils wound around a cylindrical tube of length 20 cm, in which a magnet moves from one end to the other when tilted. Their field test of the energy harvesters mounted on reindeers was of limited success as the optimum mounting position and method had not been determined a priori.

Given the above, in this paper we present the design and evaluation of a kinetic energy harvester specifically designed and tuned for mounting on wild elephants. Starting from a theoretical model adapted from [9], we then present our prototype kinetic energy harvester. The analytical model is complemented by a simulation model, and the accuracy of both models is verified experimentally in the laboratory. Using real motion data collected through our own data logger mounted on an elephant, we determine the best harvester configuration and orientation. Finally, thanks to our models and real motion data from the elephant, we estimate the amount of energy that can be harvested per day, and find that this is sufficient to perform continual monitoring of the elephant location.

The work presented in this paper is part of JumboNet [10], a collaborative effort between University of Rochester and Sri Lanka Institute of Information Technology to explore solutions to HEC using wireless communication technologies.

The rest of the paper is organized as follows. In Section II, we present the motion data collected from an elephant, which motivates the design of our energy harvester. In Section III we present the estimated energy requirements for real-time monitoring, while in Section IV we describe our energy harvester prototype and the relative analytical model. In Section V we first validate our analytical model, and then combine the analytical model with a simulation model to estimate the harvestable daily energy using the elephant motion. Finally, Section VI concludes the paper.

## II. MOTION DATA COLLECTION

In order to ascertain the possible kinetic energy harvesting opportunities on an elephant, a preliminary study of elephant motion was conducted on a domestic elephant that is engaged in carrying tourists on elephant-back tours. A domestic elephant was chosen for this purpose due to a number of reasons. First, it is easier and safer to mount and dismount any data logging equipment on a domestic elephant. Second, the activities of the elephant can more easily be monitored and recorded compared to a wild elephant. The elephant chosen for the study was 8 feet tall with front leg height of 5 feet and 4 inches. The width of the elephant at the maximum point was 5 feet. The age of the elephant was between 45 and 50 years.



Figure 1. Motion logger mounted on an Elephant.

*1) Data Logging:* A battery powered data logger was designed for storing motion and location data based on the ARM Cortex M4 microcontroller. The motion data was sensed at 10 samples per second using an MPU-9150 9-axis motion sensor, while the location data was recorded using Linx FM Series GPS module every 20s. The collected data was stored on an SD memory for later analysis. The logger was placed on a waterproof diecast aluminum enclosure that was mounted on the elephant using a leather belt, as shown in Figure 1. The data logging took place for 10 days from 10<sup>th</sup> to 17<sup>th</sup> of January 2016. During three days out of ten, the elephant activities were observed and recorded manually in order to observe any correlation between the activities and patterns in the data.

*2) Data Analysis:* Out of the ten days, two days were affected by mounting, battery charging and dismounting activities. One day was affected by shifting of the logger from the top of elephant's neck to a side. As a result, only the remaining seven days of data were used for analysis. For ease of referencing, the lateral, longitudinal and vertical axes are identified as *X*, *Y* and *Z*, respectively.

The elephant engages in walking, eating, sleeping and bathing in addition to idling during the course of the day. Out of these activities, walking, sleeping and idling were the most frequent and regular activities, and their characteristics are shown in Figure 2. Sleeping was characterized by inactivity on all three axes, while walking was characterized by periodic accelerations on all three axes. However, idling shows movement on the *Z* axis only, due to the vertical head movement of the elephant. Eating was similar to idling with only *Z* axis movements with higher amplitudes and shorter bursts.

For the rest of the analysis, the entire dataset was divided into walking and non-walking data. Using time domain features, GPS coordinates and manual records of activities, a walking data set of 52 hours and 47 minutes was extracted, averaging 6 hours and 36 minutes per day.

First, a frequency domain analysis was performed in order to identify the frequency spectrum of walking and non-walking data, as shown in Figure 3(a). From the frequency spectrum, it is clear that the bulk of the frequencies are between 0Hz and 2.5Hz, with clear peaks for all three axes around 0.33Hz-

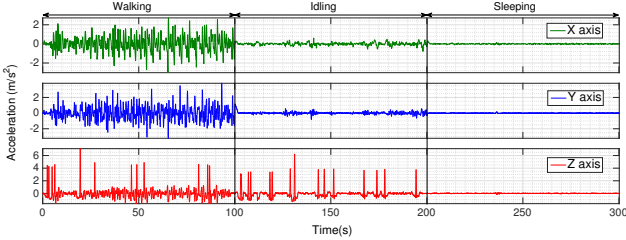
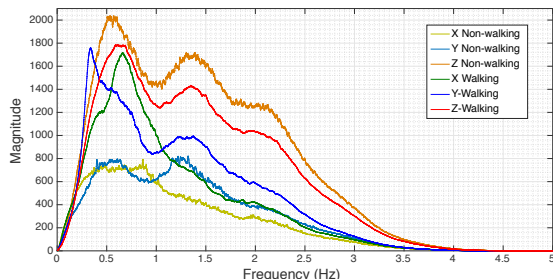
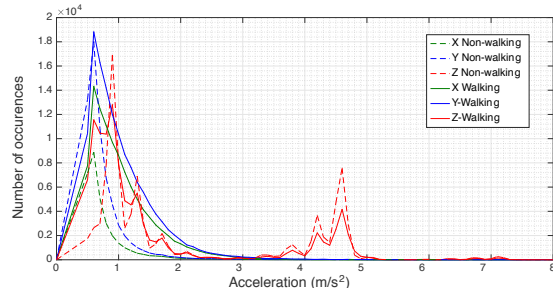


Figure 2. Time domain features of regular activities.



(a) Frequency spectrum.



(b) Peak acceleration vs. number of occurrences.

Figure 3. Frequency spectrum and peak acceleration vs. number of occurrences of walking and non non-walking data.

0.36Hz and 0.90Hz-0.98Hz. A further peak was observable around 1.50Hz-1.52Hz for the  $Y$  and the  $Z$  axes only. One unique feature in the  $Z$  axis is the higher availability of frequencies between 1Hz to 2.5Hz compared to both the  $X$  and  $Y$  axes. In addition, in the  $Z$  axis the non-walking data has a higher magnitude compared to walking data.

Next, the acceleration amplitude spectrum was plotted as shown in Figure 3(b), to identify the frequently available amplitudes, as the harvester design should be based on both frequency and amplitude of acceleration available. All three axes display a peak close to  $0.6\text{ms}^{-2}$ , with the  $Y$  axis having the highest peak, and both the  $X$  and  $Y$  axes tapering off rapidly to 1/10th of the peak at  $2\text{m/s}^2$ . However, it is interesting to note that the  $Z$  axis has the highest peak at  $0.9\text{m/s}^2$  and a significant peak at  $4.6\text{m/s}^2$ . Similar to the observation in frequency domain, the  $Z$  axis has a higher number of occurrences of non-walking accelerations than walking accelerations at the same magnitude except at  $0.6\text{m/s}^2$ .

The data presented in this section shows that the elephant

Table I  
SPECIFICATIONS OF POTENTIAL WIRELESS SENSOR MOTE SOLUTIONS

	TI CC1310 with builtin RF Radio [11]	Zolertia RE-Mote with onboard TI CC1200 RF Radio [12]
CPU/MCU	TI CC1310	ARM Cortex-M3
CPU Clock	48MHz	16MHz
Comm. Frequency	868MHz	868MHz
Range (line of sight)	$\sim 24\text{km}$	$\sim 24\text{km}$
Sensitivity	-124dBm	-123dBm
Operating Voltage	3V	3.6V
MCU Idle	$1.8\mu\text{W}$	$4.68\mu\text{W}$
Comms. System Idle	incl. in MCU idle	$0.432\mu\text{W}$
MCU Active Power	$8.1\text{mW}$	$25.2\text{mW}$
Power for Tx	$67.2\text{mW}$	$165.6\text{mW}$
Power for Rx	$16.5\text{mW}$	$84.6\text{mW}$

Table II  
U-BLOX MAX-M8 POSITIONING MODULE SPECIFICATIONS [13]

Parameter	Value
Sensitivity	-160dBm
Time for First Fix (cold start)	26s
Time for aided-start	2s
Chosen Operating Voltage	3V
Power for Acquisition	81mW
Power Save Mode (idle)	$45\mu\text{W}$

daily motion exhibits a continuous motion pattern that can be opportunistically used for kinetic energy harvesting, even during non-walking activities. This data first motivates the design of the kinetic energy harvester presented in Section IV, and is then used in Section V to finely tune the parameters of the harvester and estimate the average daily energy that can be harvested when mounted on an elephant.

### III. ENERGY REQUIREMENTS FOR REAL-TIME MONITORING

In order to estimate the minimum amount of energy required to support a real-time monitoring system that provides hourly location updates, similar to that in [3], a simple network model with direct source to sink transmission is assumed. In particular, we assume a bitrate of 1kbps, that each position update requires the transmission of 256bits, and is followed by an 80bits acknowledgement.

Two possible sensor mote solutions were considered for the purpose of estimation, as shown in Table I. In order to obtain the geographic location of the elephant, a u-blox MAX-M8 [13] positioning module could be coupled to both these solutions. This positioning module is able to retain the ephemeris data obtained after a successful cold-start for subsequent aided-starts for up to 4 hours. The energy overhead in operating in this mode is significantly lower compared to resorting to cold-start for each acquisition. The key specifications of the positioning module are summarized in Table II.

Since direct source to sink transmission is assumed, it is desirable to have a longer range in order to support a larger number of elephants with a lower number of data sinks. Therefore, an optional TI CC1190 [14] range extender could be

Table III  
TI CC1190 RANGE EXTENDER SPECIFICATIONS [14]

Parameter	Value
Output Power	26.5dBm
Chosen Operating Voltage	3V
Power for Tx	906mW
Power for Rx	9mW
Power Save Mode (idle)	0.15μW

Table IV  
ESTIMATED ENERGY BUDGET PER DAY FOR HOURLY POSITION TRANSMISSIONS

	TI CC1310 [11]	Zolertia RE-Mote [12]
MCU active + System idle	1.71J	5.24J
Wireless (Tx + Rx)	0.43J	1.15J
Position Acquisition (u-blox MAX-M8)	19.44J	19.44J
TI CC1190 Range Extender (Optional)	(5.47J)	(5.47J)
Total Energy Budget / day (with range extender)	21.59J (27.06J)	25.83J (31.30J)
Extra update with aided-start (with range extender)	0.20J (0.43J)	0.26J (0.49J)

coupled to both solutions in Table I, which offers a tested range of more than 114km line-of-sight [15]. The specifications of the range extender are summarized in Table III.

The energy required for the CPU, wireless radio, positioning module and the optional range extender for 24 position updates per day is summarized in Table IV. It is clear that position acquisition consumes 62% to 71% of the total energy budget in all considered solutions. In calculating the energy required for position acquisition, 3 aided-starts have been assumed subsequent to a cold-start. However, in optimum conditions, 4 aided-starts should be possible.

The estimated energy budget presented in this section will be used to scale the kinetic energy harvester prototype presented in Section IV, as discussed in Section V.

#### IV. KINETIC ENERGY HARVESTER

In this section, we first describe our prototype kinetic energy harvester, and then present the theory behind its design. In addition, we present an analytical model that captures the interaction between the different elements of the energy harvester and discuss some of the relative design considerations. The analytical model is used to estimate the amount of harvestable energy in Section V.

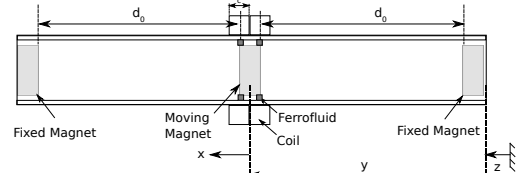
##### A. Kinetic Energy Harvester Prototype

Our prototype kinetic energy harvester (see Figure 4(a)) is based on the work presented in [9], [16], [17], which uses nonlinear oscillations of magnetic levitation for harvesting energy from the motion of magnets.

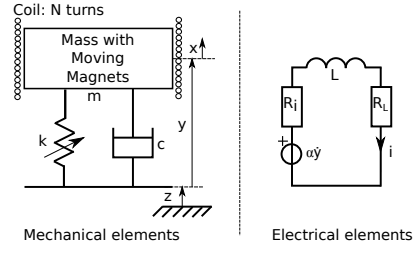
The kinetic energy harvester is composed of one moving magnet, two stationary magnets, a polycarbonate tube, and two coils. The moving magnet is made of a N42 Neodymium ring magnet of 1 inch outer diameter,  $\frac{1}{4}$  inch inner diameter



(a) Prototype.



(b) Schematic diagram.



(c) Electrical and mechanical elements [17].

Figure 4. Prototype, schematic diagram, electrical and mechanical elements of the kinetic energy harvester.

and 1 inch thickness. The moving magnet is placed inside a polycarbonate tube with inner diameter  $1\frac{1}{8}$  inches and outer diameter  $1\frac{1}{4}$  inches. The stationary magnets that are mounted on the ends of the tube are N42 Neodymium ring magnets of outer diameter  $\frac{3}{4}$  inch, inner diameter  $\frac{1}{4}$  inch and thickness  $\frac{1}{4}$  inch. The moving magnet is held in its equilibrium position at the centre of the tube by the repulsive forces exerted by the stationary magnets. This force is known as the magnetic restoring force  $F(x)$  (see, e.g., [9]). The two coils are located at the centre of the tube, and are composed of 32AWG copper wire. Each coil has 5000 turns and a resistance of  $375\Omega$ . The width of each coil is 1 inch and the mean circumference of each coil is 14.5cm.

In order to reduce the friction between the surface of the magnets and the inner surface of the polycarbonate tube, ferrofluid has been introduced to the moving magnet. Ferrofluid gets attracted to the poles of magnets and forms rings between the magnets and the inner surface of the tube, thus reducing the static coefficient of friction between the moving magnet and the polycarbonate tube from 0.5 to 0.012 [18].

Our entire energy harvester can be housed in a cylindrical enclosure of 60 mm in diameter and 150 mm in length and weighs between 525g (single coil operation) and 745g (double coil operation), excluding the weight of the enclosure that may be required for practical use.

##### B. Analytical Model

A schematic diagram of the proposed kinetic energy harvester is presented in Figure 4(b). Following the work in [9], our kinetic energy harvester prototype can be modeled as

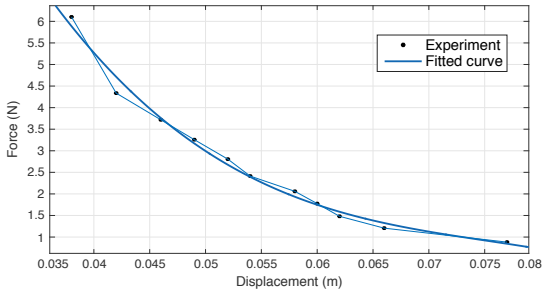


Figure 5. Magnetic repulsion force vs. separation distance.

a Single Degree of Freedom (SDOF) mass-spring-damper system with  $m$  being the moving mass,  $k$  being the stiffness of the spring and  $c$  being the damping constant, as shown in Figure 4(c). In what follows, we characterize the interaction between the different components of the energy harvester and present the system parameters of our prototype.

Assuming a linear restoring force exerted by the stationary magnets, the equation of motion of the moving magnet with mass  $m$  can be expressed as:

$$m\ddot{x} = -c(\dot{x} - \dot{z}) - k(x - z) - mg, \quad (1)$$

where  $x, \dot{x}, \ddot{x}$  are the displacement, velocity and acceleration of the moving magnet with respect to the equilibrium position of the moving magnet, respectively, while  $z, \dot{z}, \ddot{z}$  are displacement, velocity and acceleration externally applied on the housing, respectively. Here,  $g$  is the gravitational acceleration if the harvester is oriented vertically, or zero if the harvester is oriented horizontally. As shown in Figure 9, since  $x = z + y$ , Eq. (1) can be re-arranged as:

$$-m\ddot{z} = m\ddot{y} + c\dot{y} + ky + mg. \quad (2)$$

1) *Non-linear Stiffness*: In order to determine the non-linear nature of the magnetic levitation system behind our prototype, in Figure 5 we plot the repulsive force  $F(s)$  vs. distance  $s$  between the poles of a single stationary magnet and the moving magnet. To simplify the model, the experimental measurements in Figure 5 are fitted to a 3-terms power series

$$F(s) = \sum_{n=0}^3 \alpha_n s^n, \quad (3)$$

where  $s$  is the separation distance.

Considering the separation distance as a function of displacement of the centre magnet  $x$  and the spacing between the magnets in equilibrium  $d_0$ , the force displacement relationship of the left stationary magnet  $F_L(x)$  and the right stationary magnet  $F_R(x)$  can be used to express the total restoring force acting on the moving magnet stack as:

$$F(x) = F_R(x) - F_L(x) \quad (4)$$

By substituting  $d_0 + x$  and  $d_0 - x$  for  $s$  in Eq. (3), it is possible to obtain  $F_R(x)$  and  $F_L(x)$ , respectively. Then Eq. (4)

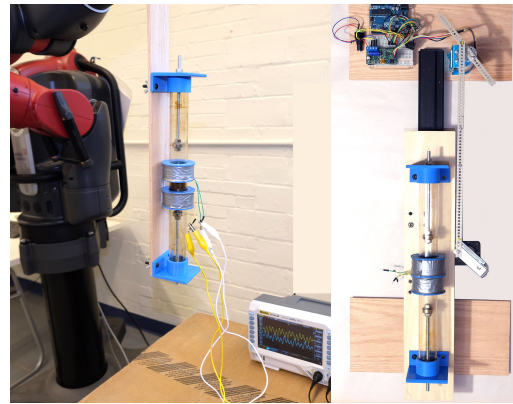


Figure 6. Left: Prototype tested vertically using the Baxter Robot. Right: Top view of the linear motion testbed.

yields  $F(x) = k(x) + k_3 x^3$ , where  $k = 2\alpha_1 + 4d_0\alpha_2 + 6d_0^2\alpha_3$  is the linear stiffness coefficient and  $k_3 = 2\alpha_3$  is the non-linear stiffness coefficient. In particular, for our prototype harvester, the experimental values are:  $\alpha_1 = 444.2\text{N/m}$ ,  $\alpha_2 = -4947\text{N/m}^2$  and  $\alpha_3 = 4302\text{N/m}^3$ . Moreover, at  $d_0 = 0.04709\text{m}$ , we obtain a linear stiffness  $k = 13.82\text{N/m}$ , and a non-linear stiffness  $k_3 = 8604\text{N/m}^3$ .

As described in [9], since the mass  $m$  of the moving magnet is known, it is possible to obtain the natural frequency  $\omega_n$  of the harvester as

$$\omega_n^2 = \frac{1}{m}(k + 3k_3 x_e^2), \quad (5)$$

where  $x_e$  is the displacement at the static equilibrium. While  $x_e = 0$  when the harvester is horizontal,  $x_e$  is non-zero when vertical as the gravitational force pushes the moving magnet down from the centre position.

When operating horizontally, Eq. (5) reduces to  $\omega_n = \sqrt{(k/m)}$ . This produces the linear resonance frequency  $f_n$ , where  $f_n = \frac{\omega_n}{2\pi}$ . For the case of our prototype, we obtain  $f_n = 1.97\text{Hz}$ , given that  $m = 0.090\text{kg}$ . When operating vertically, instead,  $x_e = 0.006\text{m}$ , which yields  $f_n = 2.03\text{Hz}$ .

2) *Electro-magnetic Damping*: Up to this point, the system was studied without an electrical load. When there is a resistive load  $R_L$  across the coil with internal resistance  $R_i$ , the current  $i$  flowing through the coil produces an opposing force to the motion generating a damping effect. If any inductance ( $L$ ) is neglected due to low frequency operation, then Kirchoff's law yields  $i(R_L + R_i) - \alpha(\dot{x} - \dot{z}) = 0$ , where  $\dot{x} - \dot{z} = \dot{y}$ , and  $\alpha = NBl$  represents the electromechanical coupling coefficient. Here,  $N$  is the number of turns,  $l$  is the length of the coil per turn and  $B$  is the average magnetic field strength. Using the above, Eq. (2) of motion can be re-written as:

$$-m\ddot{z} = m\ddot{y} + (c_m + c_e)\dot{y} + ky + k_3 y^3 + mg, \quad (6)$$

where  $c_e = \frac{\alpha^2}{R_i + R_L}$  represents the electrical damping coefficient and  $c_m$  represents the mechanical damping coefficient.

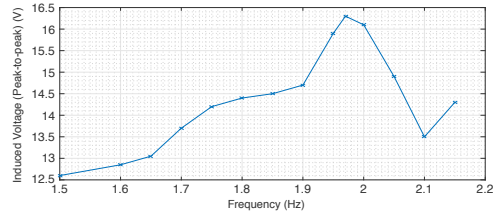


Figure 7. Harvester output (without load) at constant displacement.

Table V  
SIMULATION MODEL PARAMETERS

Parameter	Value	Parameter	Value
$m$	0.09kg	$c_m$ (Vertical)	0.024Ns/m
$d_0$	0.04709m	$c_m$ (Horizontal)	0.048Ns/m
$k$	13.82N/m	$\alpha$	{6.5, 7.7, 8.9} Vs/m
$k_3$	8604N/m	$R_i$	375Ω
$f$	1.97Hz	$A$	3.251m/s <sup>2</sup>

## V. NUMERICAL RESULTS

### A. Experimental and Simulation Setup

In order to validate the model presented in Section IV-B, we evaluated the performance of our prototype kinetic energy harvester on two test environments. The first test environment uses a geared DC motor controlled by an Arduino Uno to generate a simple linear motion (see Figure 6). Using a sliding platform and a crank attached to the motor, an oscillatory linear motion was produced with adjustable displacement, velocity and acceleration. Using this environment, we first determined the resonance frequency by varying the frequency of the back and forth linear motion of the horizontal sliding platform, while maintaining the displacement amplitude at 20mm. The output of this experiment is shown in Figure 7. We note that resonance occurred at 1.97Hz, which is in agreement with the natural frequency derived in Eq. (5).

The second test environment is represented by a Baxter research robot, as shown in Figure 6. Using the robot, we were able to re-produce the real elephant motion based on the velocity and displacement data for both the vertical and horizontal orientations.

In addition to the experimental settings described above, we developed a simulation model in MATLAB Simulink to simulate the motion of the moving magnet and to obtain the relative induced voltage on each coil (i.e., Eq. (6)). This model consider a single magnet and a single coil, as shown in Figure 8, and provides the induced voltage on the coil as a function of a given external excitation.

The simulator was operated in two modes. First, a known external acceleration  $A \sin(\omega t)$ , where  $A$  represents the amplitude of acceleration,  $\omega$  is the angular velocity and  $t$  is time, was provided as the input. The induced voltage was recorded for a range of load resistances  $R_L$ . Second, for a chosen  $R_L$  for which maximum power transfer occurs ( $R_{MPT}$ ), the recorded accelerations from the elephant motion were provided as the input. In this case, the energy transferred to the load for the acceleration along each axis and each day were determined.

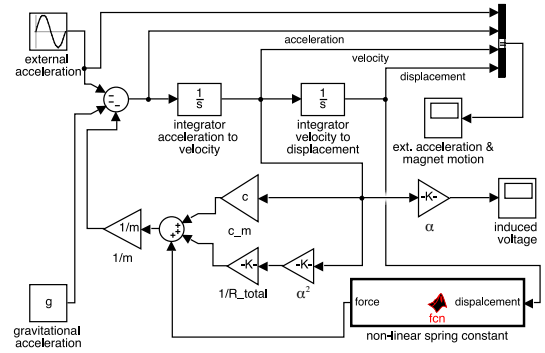
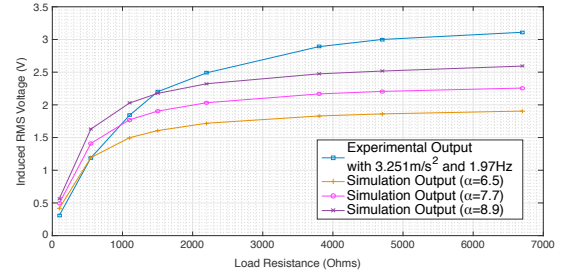
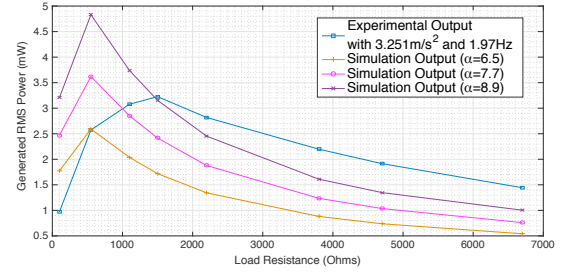


Figure 8. MATLAB Simulink model.



(a) Induced voltage (RMS) vs. load resistance.



(b) Power generated (RMS) vs. load resistance.

Figure 9. Induced voltage (RMS) and power generated (RMS) as a function of the load resistance.

The simulation model parameters are listed in Table V.

### B. Experimental Results and Discussion

The responses of both the experiment and the simulation for varying load resistance while operating at resonance frequency with constant acceleration are shown in Figure 9(a). These results were then used to determine the maximum power transfer point  $R_{MPT}$ . The RMS power vs. load resistance plot is shown in Figure 9(b). From the plot,  $R_{MPT} = 1500\Omega$ .

In order to estimate the daily energy generation,  $\alpha$  must be chosen so that the simulation matches the RMS power generated from the experiment at  $R_{MPT}$ . According to our experimental results, we set  $\alpha = 8.9$ . The estimated daily energy generation, when using the elephant motion data presented in Section II, is shown in Table VI and provide a clear choice for the orientation of the energy harvester. In particular, operating the harvester vertically, along the Z axis, generates the most amount of energy (88.91J, on average). Moreover, as

Table VI  
DAILY ENERGY GENERATION FOR ACTUAL MOTION DATA

	Energy Transferred to Load (J)		
	X axis	Y axis	Z axis
Day 1	5.31	9.75	80.92
Day 2	8.75	13.78	81.04
Day 3	5.49	11.05	84.65
Day 4	6.95	13.16	81.13
Day 5	6.09	11.93	88.82
Day 6	10.96	22.2	88.14
Day 7	5.00	9.46	117.70
Average	6.94	13.05	88.91

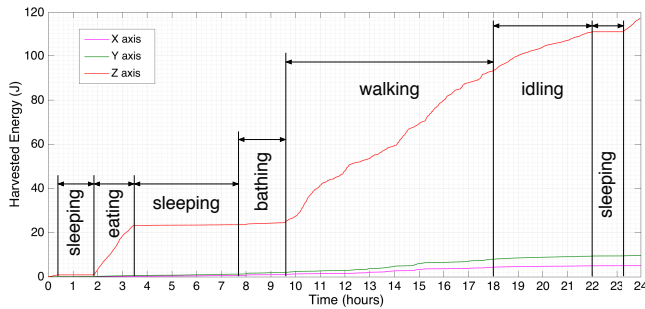


Figure 10. Estimated energy generation on day 7.

shown in Figure 10, a considerable amount of energy can be generated even during non-walking activities.

Although dual coil operation did not improve the total harvested energy significantly compared to a single coil, it may be useful to have dual coils for efficient rectification and harvester circuit design. However, a second coil adds 220g of weight to the energy harvester.

Finally, we note that the use of electromagnetic coupling coefficient  $\alpha$  in the analytical model ignores the relative position of the moving magnet and the coil. In practice, the magnetic flux density of the magnet is not constant throughout its length axis. Nevertheless, during our experiments we observed that, within the range of accelerations recorded on the elephant, the relative displacement between the magnet and the coil is less than half the length of the magnet. Therefore, this approximation does not adversely affect the final result.

As shown in Table VI, when using the elephant vertical motion, our prototype energy harvester is able to generate a daily average of 88.91J before rectification, DC-DC conversion and storage. Using modern technologies, these operations have an aggregate efficiency greater than 75% (see e.g., [19]), thus bringing the useful energy to at least 66.7J per day. Thus, our proposed prototype is able to support the requirements for real-time monitoring described in Section III. As an example, when using a TI CC1310 with the optional range extender, the total energy consumption required for acquiring one GPS reading per hour is 27.06J, which provides a surplus energy of 39.64J. This additional energy can therefore be used, for example, for increasing the frequency of position updates or to support a GPRS-based communication (estimated as 5.1J per update when using, e.g., the SIM908 GPRS module [20]).

## VI. CONCLUSIONS

In this paper, we introduced a kinetic energy harvester that can be used to power elephant mounted tracking units (tags). This eliminates the need for tracking units that have limited life spans due to limited battery capacity. Using a simulation developed based on an analytical model, and motion data recorded on an elephant, we showed that the proposed harvester is able to generate an average of 88.91J per day, which can support 24 transmissions of locations per day up to a maximum distance of 114km line of sight. Even with the highest estimated energy budget (as presented in Table IV), our prototype energy harvester provides a daily surplus of 35.40J that can be used to increase the frequency of position updates or to support alternative communication options such as GPRS. Therefore, our proposed approach represents a viable method to support WSN-based real-time monitoring of elephants.

## REFERENCES

- [1] IUCN. (2016) IUCN red list of threatened species. [Online]. Available: <http://www.iucnredlist.org/details/7140/0>
- [2] P. Fernando, J. Jayewardene, and T. Prasad, "Current status of Asian elephants in Sri Lanka," *Gajah*, 2011.
- [3] J. Wall, G. Wittemyer, and B. Klinkenberg, "Novel opportunities for wildlife conservation and research with real-time monitoring," *Ecological Applications*, 2014.
- [4] P. Juang, H. Oki, Y. Wang, M. Martonosi, L. S. Peh, and D. Rubenstein, "Energy-efficient computing for wildlife tracking: Design tradeoffs and early experiences with zebrafish," *SIGOPS Oper. Syst. Rev.*, 2002.
- [5] A. Balasubramanian, "Architecting protocols to enable mobile applications in diverse wireless networks," Ph.D. dissertation, University of Massachusetts, Amherst, 2011.
- [6] K. Soulsby, "Use of a tri-axial accelerometer, behavioral observation, and gps to monitor the activity of female asian elephants in a zoo," Master's thesis, The University of Texas at Arlington, Arlington, 2013.
- [7] Z. E. Rowell, "Locomotion in captive Asian elephants (*Elephas maximus*)," *Journal of Zoo and Aquarium Research*, vol. 2, no. 4, pp. 130–135, Oct. 2014.
- [8] A. Gutierrez, N. I. Dopico, C. Gonzalez, S. Zazo, J. Jimenez-Leube, and I. Raos, "Cattle-Powered Node Experience in a Heterogeneous Network for Localization of Herds," *IEEE Trans. Ind. Electron.*, vol. 60, no. 8, pp. 3176–3184, Apr. 2013.
- [9] B. P. Mann and N. D. Sims, "Energy harvesting from the nonlinear oscillations of magnetic levitation," *Journal of Sound and Vibration*, vol. 319, no. 1-2, pp. 515–530, Jan. 2009.
- [10] "JumboNet." [Online]. Available: <http://www.jumbonet.lk>
- [11] CC1310 - Sub-1 GHz Ultra-Low Power Wireless Microcontroller, Texas Instruments, 10 2015, rev. B.
- [12] Zolertia RE-Mote Hardware Development Platform, Zolertia, 12 2015.
- [13] u-blox M8 concurrent GNSS module, ublox, 11 2015, rev. 10.
- [14] CC1190 850-950MHz RF Front End, Texas Instruments, 02 2010.
- [15] R. Wallace. (2015, Mar.) Achieving Optimum Radio Range. [Online]. Available: <http://www.ti.com/lit/an/swra479/swra479.pdf>
- [16] E. Dallago, M. Marchesi, and G. Venchi, "Analytical Model of a Vibrating Electromagnetic Harvester Considering Nonlinear Effects," *IEEE Trans. Power Electron.*, vol. 25, no. 8, pp. 1989–1997, Jun. 2010.
- [17] P. L. Green, E. Papatheou, and N. D. Sims, "Energy harvesting from human motion and bridge vibrations: An evaluation of current nonlinear energy harvesting solutions," *Journal of Intelligent Material Systems and Structures*, vol. 24, no. 12, pp. 1494–1505, Aug. 2013.
- [18] J. T. Cheung, "Frictionless linear electrical generator for harvesting motion energy," DTIC Document, Tech. Rep., 2004.
- [19] D. Maurath, C. Peters, T. Hehn, M. Ortmanns, and Y. Manoli, "Highly efficient integrated rectifier and voltage boosting circuits for energy harvesting applications," *Advances in Radio Science*, vol. 6, no. D. 3, pp. 219–225, 2008.
- [20] "SIMCOM SIM908." [Online]. Available: <http://www.simcom.ee/modules/gsm-gprs-gps/sim908/>